

# Journal of Materials Chemistry A

Accepted Manuscript



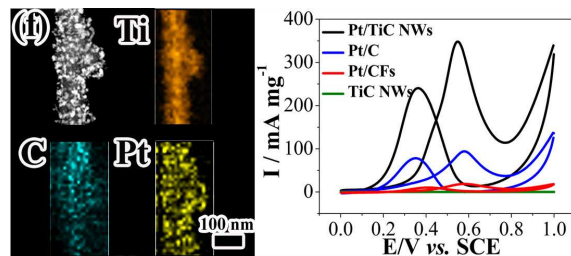
This is an *Accepted Manuscript*, which has been through the Royal Society of Chemistry peer review process and has been accepted for publication.

*Accepted Manuscripts* are published online shortly after acceptance, before technical editing, formatting and proof reading. Using this free service, authors can make their results available to the community, in citable form, before we publish the edited article. We will replace this *Accepted Manuscript* with the edited and formatted *Advance Article* as soon as it is available.

You can find more information about *Accepted Manuscripts* in the [Information for Authors](#).

Please note that technical editing may introduce minor changes to the text and/or graphics, which may alter content. The journal's standard [Terms & Conditions](#) and the [Ethical guidelines](#) still apply. In no event shall the Royal Society of Chemistry be held responsible for any errors or omissions in this *Accepted Manuscript* or any consequences arising from the use of any information it contains.

## Graphical Abstract



## Highlight

The unique one-dimensional bark-structured TiC NWs possess high electrical conductivity, excellent chemical/electrochemical stability, enhancing electrocatalytic properties.

# Biotemplated synthesis of bark-structured TiC nanowires as Pt catalyst support with enhanced electrocatalytic activity and durability for methanol oxidation

Cite this: DOI: 10.1039/x0xx00000x

Received 00th January 2014,

Accepted 00th January 2014

DOI: 10.1039/x0xx00000x

[www.rsc.org/](http://www.rsc.org/)

Zhen Qiu, Hui Huang\*, Jun Du, Xinyong Tao, Yang Xia, Tong Feng, Yongping Gan, Wenkui Zhang\*

Developing Pt electrocatalysts with high activity and long-term durability remains a great challenge for commercializing fuel cells. Herein, we report a new kind of bark-structured TiC nanowires (NWs) as an efficient support for Pt electrocatalysts, which exhibits higher electrochemical active surface area (ECSA), much improved electrocatalytic activity and long-term durability toward methanol oxidation reaction (MOR) when compared with commercial Pt/C (Vulcan XC-72) catalysts. The TiC NWs were synthesized *via* a simple biotemplating method using natural nanoporous cotton fibers as both the carbon source and the template. And their typical size is in the range of 50–150 nm in width and up to several micrometers in length. The Pt nanoparticles deposited onto the TiC NWs by urea-assisted ethylene glycol reduction method are small (*ca.* 3 nm), narrowly distributed and well crystallized. The unique one-dimensional (1D) nanostructures of TiC NWs provide fast transport and short diffusion paths for electroactive species and high utilization of catalysts. Moreover, the merits of TiC NWs such as high electrical conductivity, excellent chemical/electrochemical stability also contribute to enhancing electrocatalytic properties. The carbide support reported here will promote broader interest in the further development of Pt electrocatalysts in the fields of fuel cells and related electrocatalytic applications.

## 1 Introduction

Developing highly efficient electrocatalyst at low cost still remains a significant technical challenge for the commercialization of fuel cells devices.<sup>1–8</sup> It is well known that the catalyst support plays a significant role in the promotion of electrocatalytic performance and the reduction of Pt usage.<sup>9–11</sup> To date, the most common supports for Pt electrocatalyst are carbon materials, in particular Vulcan XC-72.<sup>12–14</sup> However, the practical large-scale commercialization of fuel cells is severely limited because of the loss of electrochemical active surface area (ECSA) and the decrease of catalytic activity over time.<sup>15,16</sup> Moreover, carbon materials are vulnerable to corrosion/oxidation at high potentials (>0.7 V vs NHE) under the normal operating condition, resulting in poor durability of electrocatalyst because of the dissolution, Ostwald ripening, and aggregation.<sup>14, 17–19</sup> The low polarity and high hydrophobicity features of carbon are also identified as major drawbacks to limit rate performance of carbon-supported catalysts.<sup>5</sup> Therefore, the development of catalyst supports

with improved activity and durability of Pt catalyst is highly desirable.

Recently, carbides as supports have aroused increasing interest because of their high chemical and thermal stability, outstanding anti-corrosion ability and low electrical resistivity.<sup>14, 20</sup> It has been reported that carbide-supported electrocatalysts are highly active for both the oxygen reduction reaction (ORR) and methanol oxidation reaction (MOR) due to electrocatalytic synergistic effect and their Pt-like behavior for electrocatalysis.<sup>6, 21–23</sup> Wang and co-workers<sup>24</sup> found that core-shell structured SiC@C supported platinum catalysts in direct methanol fuel cells (DMFCs) achieved high durability and catalytic performance. Grubb and McKee<sup>25</sup> investigated commercial boron carbide (B<sub>4</sub>C) powder supported Pt as an anode material in phosphoric acid fuel cells (PAFCs), exhibiting an enhancement of the Pt activity. Mu and co-workers<sup>11</sup> reported that B<sub>4</sub>C nanoparticles supported Pt catalysts presented much enhanced methanol oxidation activity and CO tolerance in comparison to Pt/C catalysts. These improved MOR activity and electrochemical stability result from their excellent corrosion resistance and oxidative stability of SiC and B<sub>4</sub>C.<sup>11, 24, 25</sup> However, SiC and B<sub>4</sub>C belong to covalent carbide, where the carbon atoms are bonded to the Si or B atoms by sharing a pair of electrons.<sup>26</sup> Their low electrical conductivity constitutes a major obstacle for their practical application fuel cells. Therefore,

College of Chemical Engineering and Materials Science, Zhejiang University of Technology, Hangzhou, 310014, P. R. China. E-mail: [hhui@zjut.edu.cn](mailto:hhui@zjut.edu.cn); [msechem@zjut.edu.cn](mailto:msechem@zjut.edu.cn); Tel: +86-571-88320394

† Electronic supplementary information (ESI) available. See DOI: TA-ART-01-2014-000277

transition metal carbides (TMC) are of special interests due to their properties of superior electrical conductivity and good chemical stability.<sup>14</sup> Gogotsi *et al.*<sup>27</sup> have reported titanium carbide MXenes have shown promise as electrode materials.

In addition, the control on support material structures provides a sensitive knob to tune the properties and improve the functions. To this end, one-dimensional (1D) nanostructures, such as nanowires, represent an important research direction because 1D nanostructures exhibit improved surface chemistry and catalytic properties.<sup>28-30</sup> Chan *et al.*<sup>31</sup> designed carbon-coated TiO<sub>2</sub> fibers as electrocatalyst support for methanol oxidation, suggesting higher catalytic activity and better stability than Pt-C. Lee and co-workers<sup>32</sup> reported that well-aligned mesoporous carbon nanowires (MCNWs) as the support material for Pt electrocatalyst presented better catalytic performance than commercial Pt/Vulcan XC-72, which attributes to the good dispersion of Pt and a special morphology of MCNWs. Chu *et al.*<sup>33</sup> have also demonstrated a promising electrocatalyst for methanol oxidation based on a novel PtPd/C nanowire networks with both outstanding catalytic activity and durability. The main achievement is the improvement of durability with the formation of nanowire structure. The previous studies revealed that a 1D core/shell nanostructured Pt catalyst can combine both synergistic effects and shape effects to enhance the catalytic activity and durability.<sup>14, 34, 35</sup> Obviously, the 1D NWs leads to increased surface areas that provide more active sites and increase Pt utilization per mass.<sup>36</sup> In our recent work, highly conductive TMC nanostructures including TiC, NbC, TaC nanowires have been fabricated by a biotemplated carbon-thermal method.<sup>14, 26, 37-39</sup> In this work, we report for the first time an investigation of biotemplated synthesized bark-structured TiC NWs as the support of Pt electrocatalyst. Electrochemical measurements clearly indicate that the as-prepared Pt/TiC NWs electrocatalyst has higher MOR activity (348.3 mA mg<sup>-1</sup> Pt), long-term durability, larger ECSA (203.83 m<sup>2</sup> g<sup>-1</sup>) and higher poison-tolerance to carbonaceous species generated during MOR in comparison with the commercial Pt/C catalyst.

## 2 Experimental

### Preparation of TiC NWs

TiC NWs were prepared by a simple, convenient and cost-effective biotemplate method. In a typical experiment, 0.8 g of TiO<sub>2</sub> powders, 0.29 g of NaCl and 0.15 g of Ni(NO<sub>3</sub>)<sub>6</sub>H<sub>2</sub>O were dissolved into 50 mL of ethanol to form a Ni-Ti-Cl emulsion under ultrasound irradiation. Then, a piece of T-shirt with a weight of 1.5 g was cut and dipped in the Ni-Ti-Cl emulsion. After stirring for 1 h, the cotton textile was dried at 80 °C for 30 min in a preheated oven and finally cured at 110 °C for 2 h. The nickel-, chlorine-, and titanium-loaded cotton textile, covered with titanium slices, was placed in a sealed graphite crucible and then heated at 1200 °C at a heating rate of 5 °C/min with 350 sccm continuous flow of argon. After 3 h calcination, the furnace was turned off and allowed to cool naturally to room temperature. The carbon fabrics was synthesized *via* calcination of cotton textile, by a similar procedure as TiC NWs. The carbon fabrics and commercial Vulcan XC-72 carbon support were used for comparison.

### Preparation of Pt catalysts

For a typical urea-assisted ethylene glycol (HD-EG) synthesis,<sup>40</sup> 300 mg of urea (molar ratio of urea/Pt = 20) and 0.2 g of TiC NWs were put into 200 mL of deionized water, and sonicated for 30 min. 5 mL of 0.05 M H<sub>2</sub>PtCl<sub>6</sub>·6H<sub>2</sub>O aqueous solution was added into the mixture under slowly stirring for 1 h. Next, the mixture was heated

to 90 °C to cause urea hydrolysis for 2 h. After the mixture was slowly cooled to room temperature, 200 mL of ethylene glycol was added and stirred for 2 h, and then heated at 120 °C for 2 h under stirring conditions. Afterwards, the as-formed catalyst slurry was filtered and washed with deionized water and absolute ethanol 3–4 times, respectively, followed by drying at 80 °C for 10 h to obtain the final hybrid Pt/TiC NWs. For comparison, carbon fabrics supported Pt catalyst (Pt/CFs) and Vulcan XC-72 supported Pt catalyst (Pt/C) was synthesized by the same procedure noted above.

### Material characterizations

The structure and morphology of the sample were characterized by scanning electron microscope (SEM, Hitachi S-4800), transmission electron microscope (TEM, FEI Tecnai G2 F30) and high resolution TEM (HRTEM) equipped with an energy dispersive X-ray spectroscopy (EDS) detector. The phase purity and crystalline structure of the TiC NWs were analyzed by X-ray diffraction (XRD) using an X' Pert Pro diffractometer with Cu K $\alpha$  radiation ( $\lambda=0.15418$  nm). The chemical state analysis of Pt in the catalyst was carried out by X-ray photoelectron spectroscopy (XPS) using an ECSALAB 250 X-ray photoelectron spectrometer.

### Electrocatalytic measurements

For preparing the test electrode, 2 mg of the as-prepared Pt/TiC NWs, Pt/CFs and Pt/C catalyst was dispersed into 1 mL of deionized water, respectively. After 1 h ultrasonication, 20  $\mu$ L of the catalyst slurry was transferred to the flat surface of a glassy carbon electrode (5 mm diameter) by a microsyringe. Finally, 5  $\mu$ L of 0.1 wt% Nafion solution was pipetted onto the catalyst film and dried at room temperature.

Cyclic voltammetry (CV) and chronoamperometry (CA) tests were performed in an electrolyte of 0.1M H<sub>2</sub>SO<sub>4</sub> + 1.0 M CH<sub>3</sub>OH, using the electrochemical workstation (CHI650b) in a typical three-electrode cell at room temperature. The modified glassy carbon electrode was used as the working electrode and a Pt foil was used as the counter electrode. All potentials in this study are referenced to the saturated calomel electrode (SCE). The CVs were measured in the potential range of 0–1.0 V at a scan rate of 20 mV s<sup>-1</sup>, while CA was performed at a given potential of 0.6 V. The ECSA of Pt in the catalyst was determined by hydrogen adsorption/desorption charge (Q<sub>H</sub>) between -0.25 and 0.05 V (*vs* SCE) through CV measurements, which were recorded from -0.25 to 1.0 V in 0.5 M H<sub>2</sub>SO<sub>4</sub> solution at a scan rate of 50 mV s<sup>-1</sup>. Here, the Q<sub>H</sub> was estimated by using the expression, Q<sub>H</sub> = 0.5 × (Q<sub>total</sub> - Q<sub>DL</sub>), where Q<sub>total</sub> is the total charge transfer in the hydrogen adsorption/desorption potential region and Q<sub>DL</sub> is the charge from double-layer charging of Pt and the support.<sup>18</sup>

## 3 Results and discussion

Fig. 1a, b shows the low/high-magnification SEM images of the TiC NWs. The as-prepared product is composed of abundant nanowires with the width of 50-150 nm and the length of larger than 2  $\mu$ m, respectively. Most of the NWs are straight but the surface appears a little coarser. The TEM images clearly show that the TiC NWs have an interesting bark-like structure (Fig. 1c, d). The HRTEM images of the inside and outside regions taken from an individual TiC NW in Fig. 1d are shown in Fig. 1e, f and g. Fig. 1e shows that the *d*-spacing value of the adjacent lattice fringes is 0.22 nm, corresponding well to the spacing of the (200) planes of cubic TiC. Fig. 1g presents the magnified HRTEM image of the selected region in Fig. 1f. The spacing between two adjacent lattice fringes is 0.22 nm, consisting well with the (200) planes of cubic TiC (JCPDS 65-8807), which further indicates the successful fabrication of the bark-

structured TiC NWs. On the basis of the above HRTEM results (Fig. 1e, g), it can be concluded that the inside and outside region of the bark-like structure TiC NWs have the same crystallographic orientation. The high-angle annular dark-field scanning TEM (HAADF-STEM) image of a single TiC NW and the corresponding elemental mappings reveal that the Ti and C elements were uniformly distributed within the NW (Fig. 1h-j). Fig. 1k shows the XRD pattern of the TiC NWs, in which five characteristic diffraction peaks are observed. The reflections of the cubic TiC (Fm3m) at  $31.0^\circ$ ,  $41.9^\circ$ ,  $60.7^\circ$ ,  $72.7^\circ$ ,  $76.5^\circ$  are indexed to the (111), (200), (220), (311), and (222). No  $\text{Ti}_x\text{O}_y$ ,  $\text{TiO}_x\text{C}_y$  and Ti phases were detected, suggesting that  $\text{TiO}_2$  was successfully converted to TiC.<sup>37</sup>

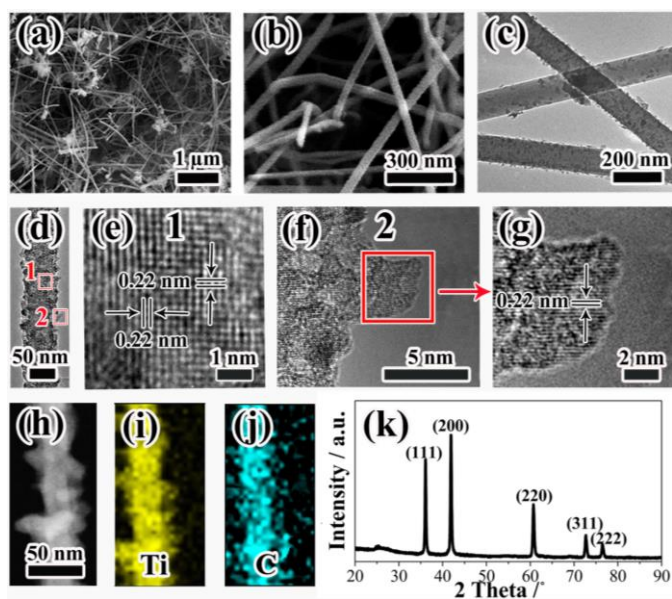


**Fig. 1** (a) Typical low-magnification and (b) high-magnification SEM images of TiC NWs. (c) TEM images of TiC NWs. (d) TEM image of an individual TiC NW. (e) HRTEM image of the inside region of TiC NW. (f) HRTEM image of the outside region of TiC NW. (g) magnified HRTEM image of a part of (f). (h-j) HAADF-STEM characterization of a single TiC NW. (k) XRD patterns of TiC NWs.

Fig. 2a, b show typical low/high-magnification TEM images of the Pt/TiC NWs catalyst. It can be seen that a great number of Pt nanoparticles were deposited on the surface of TiC NWs. These Pt nanoparticles are small with the average size of 3nm (Fig. S1, see ESI). The HRTEM image indicates that the Pt nanoparticles were uniformly dispersed on TiC NWs with no obvious agglomeration (Fig. 2c). Fig. 2d, e is the magnified HRTEM images of the selected rectangular areas marked in Fig. 2c. The inset is the corresponding indexed FFT pattern. As shown in Fig. 2d, the lattice spacing values are 0.19 and 0.14 nm, corresponding well to the spacing of the (200) and (220) crystal planes of the *fcc* crystal Pt, respectively. The sharp diffraction spots also indicate that the Pt nanoparticles are single-crystalline in nature with the growth direction along [001]. In Fig. 2e, the spacing between two adjacent lattice fringes is 0.22 nm, corresponding to the spacing of the (200) crystal planes of cubic TiC, which agrees well with that revealed by Fig. 1e, g. Fig. 2f presents the elemental dispersion of C, Ti and Pt in Pt/TiC NWs. These three elements in the product were uniformly distributed in the randomly selected area, consisting well with the results in Fig. 1h-j. The interesting 1D nanostructure of TiC support, small Pt particle size and high dispersion of Pt nanoparticles may lead to high utilization efficiency of Pt and excellent electrocatalytic properties.

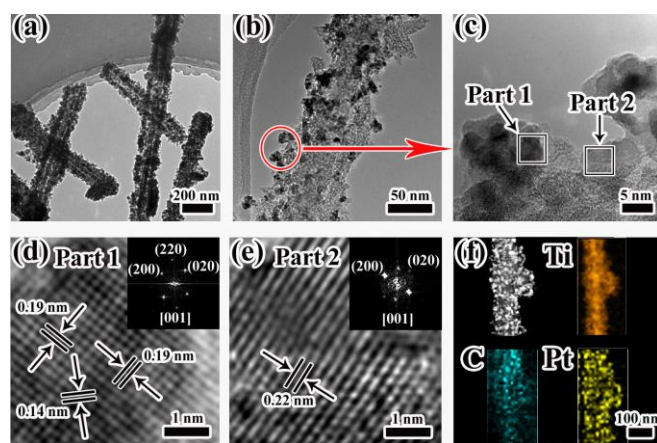


**Fig. 2** (a, b) TEM images of as-prepared Pt/TiC NWs catalysts. (c) HRTEM image. (d, e) Magnified HRTEM images of the different regions, the insets are the corresponding FFT images. (f) HAADF-STEM characterization of Pt/TiC NW.

Fig. 3 depicts the electrocatalytic performance of the Pt/TiC NWs, Pt/C and Pt/CFs catalysts, which were evaluated by CVs in electrolytes of 0.1M  $\text{H}_2\text{SO}_4$  and 1 M  $\text{CH}_3\text{OH}$  at a scan rate of  $20 \text{ mV s}^{-1}$ . In our cases, the mass activity of the Pt catalyst was adopted and defined by the peak current per amount of Pt loading. As shown in Fig. 3a, the bare TiC NWs electrode has no current peaks of methanol oxidation, suggesting that the TiC NWs have no electrocatalytic activity for MOR. While, the Pt/TiC NWs electrode shows the typical features of MOR, and the two oxidation peak potentials ( $E_p$ ) are located at 0.549 V for the forward scan and 0.358 V for the backward scan, respectively. Furthermore, the Pt/TiC NWs catalyst displays higher current density than that of the Pt/C and Pt/CFs catalysts. The forward peak current density of Pt/TiC NWs is  $348.3 \text{ mA mg}^{-1}\text{Pt}$ , which is almost 4 and 7 times higher than that of the Pt/C ( $94.1 \text{ mA mg}^{-1}\text{Pt}$ ) and Pt/CFs ( $53.5 \text{ mA mg}^{-1}\text{Pt}$ ) catalysts, respectively. The performance of the catalysts was also compared by dividing the peak current by ECSA (Fig. S3, see ESI). The forward peak current density of Pt/TiC NWs is  $1.71 \text{ A m}^{-2}\text{Pt}$ , which is  $\sim 2.5$  and  $1.6$  times higher than that of the Pt/C ( $0.69 \text{ A m}^{-2}\text{Pt}$ ) and Pt/CFs ( $1.08 \text{ A m}^{-2}\text{Pt}$ ) catalysts, respectively. These results clearly demonstrate that the Pt/TiC NWs has much higher catalytic activity than the Pt/C and Pt/CFs in terms of both mass-specific activity and area-specific activity. In addition, the onset potential of the forward anodic peak of Pt/TiC NWs is obviously lower than that of the Pt/C and Pt/CFs catalysts, indicating that the TiC NWs support is more favorable to improve the MOR kinetics by lowering the overpotential.<sup>41</sup>

The peak potential position of MOR during long-term CV scans is considered as the important parameter to evaluate the performance of electrocatalysts.<sup>42-45</sup> Fig. 3b presents the variation of the peak potential position on the forward scan with the increasing cycle number. The peak potential of the Pt/TiC NWs catalyst is obviously lower than that of the Pt/C and Pt/CFs catalysts during the whole CV processes (Fig. 3b), implying that the MOR is easier on the Pt/TiC NWs catalyst than that on the Pt/C and Pt/CFs catalysts. In addition, the ratio of the forward peak current ( $I_f$ ) to the backward peak current ( $I_b$ ) is considered to be a critical indicator to evaluate the poison tolerance of Pt-based catalysts in MOR. Generally, a higher  $I_f/I_b$  ratio indicates more effective resistance to the poisoning of reaction species on the catalyst surface.<sup>10, 44, 46, 47</sup> As shown in Fig. 3c, the initial  $I_f/I_b$  values are 1.45, 1.29, and 2.2 for Pt/TiC NWs, Pt/C and Pt/CFs, respectively. Furthermore, after 500 cycles, the  $I_f/I_b$  value of Pt/TiC NWs is 1.35, about 93.1% of its initial value, while

that of Pt/C and Pt/CFs drops to 87.6 and 75%, respectively. The above results indicate that the Pt/TiC NWs catalyst has higher MOR activity and better poison-tolerance towards reaction intermediates than the Pt/C and Pt/CFs catalysts. To further evaluate the rate of surface poisoning and the stability of the electrocatalysts, CA curves of Pt/TiC NWs, Pt/C and Pt/CFs catalysts are measured at 0.6 V in an electrolyte of 0.1 M H<sub>2</sub>SO<sub>4</sub> + 1.0 M CH<sub>3</sub>OH for 1000 s (Fig. 3d).<sup>48,49</sup> From the inset in Fig. 3d, it is obvious that the Pt/TiC NW catalyst exhibits a higher initial charging currents and a lower deterioration rate over the entire time range than the Pt/C and Pt/CFs catalysts, indicating a higher tolerance to the carbonaceous species generated during methanol oxidation. In addition, much higher current density is seen for the Pt/TiC NW catalyst in comparison with the Pt/C and Pt/CFs catalysts during the whole CA process (Fig. 3d). It also reveals that the Pt/TiC NW catalyst has much higher electroactivity and stability. TiC NWs are a highly effective support to improve the electrocatalytic performances for MOR.

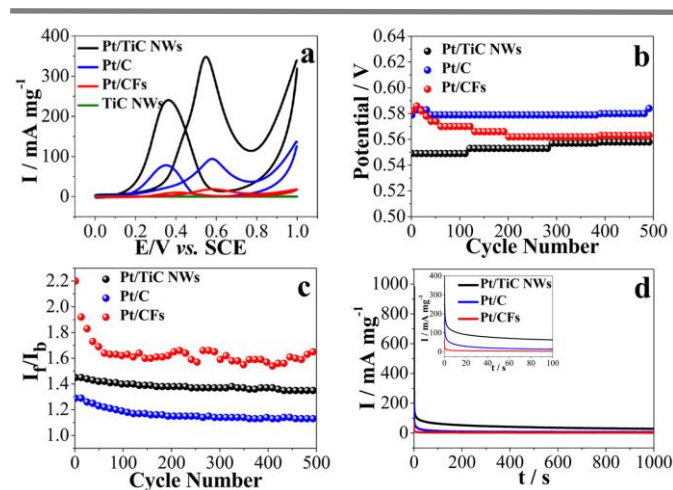


**Fig. 3** (a) CVs of the Pt/TiC NWs, Pt/C and Pt/CFs catalysts in 0.1 M H<sub>2</sub>SO<sub>4</sub> and 1.0 M CH<sub>3</sub>OH at a scan rate of 20 mV s<sup>-1</sup>. (b) Changes of peak potentials and (c) the ratio of the current density values in two sequential forward and backward sweeps (I<sub>f</sub>/I<sub>b</sub>) during the successive cycling. (d) CA curves for MOR recorded at 0.6 V, the inset Fig. is a magnification zone.

As we know, the Pt catalytic activity is not only relative to the particle size, but also depends on the interfacial interaction between Pt and the support. The TEM image of the as-prepared Pt/C (Vulcan XC-72) catalyst is presented in Fig. S2a (see ESI). The Pt nanoparticles with the average particle size of about 3 nm are uniformly dispersed on the surface of Vulcan XC-72 carbon (Fig. S2b, see ESI). As the results of TEM analysis, there is no distinctive difference in the particle size of Pt supported on TiC NWs and Vulcan XC-72 carbon. Therefore, it can be concluded that the nature of support material is a critical factor for achieving high MOR activity. Due to its excellent electrical conductivity<sup>50-52</sup> and 1D nanoarchitecture, the TiC NWs could facilitate electron transport along the long dimension and the two short dimensions provide short pathways for species.<sup>14, 26</sup> Therefore, the electron interactions between the Pt and TiC NWs can efficiently promote hydroxyl adsorption and OH<sub>ad</sub> surface coverage, resulting in a great enhanced catalytic activity for MOR.

In order to evaluate the interfacial interaction between Pt and the TiC NWs support, the XPS analysis was carried out. Fig. 4 a, b and c presents the Pt 4f XPS spectra of Pt/TiC NWs, Pt/C and Pt/CFs, respectively. The binding energies of all the peaks are determined by referencing to the C 1s value of 284.8 eV. Each Pt 4f peak can be deconvoluted into two pairs of doublets. A comparison of the relative areas of integrated intensity of Pt<sup>0</sup> and Pt<sup>2+</sup> shows that Pt<sup>0</sup> is

the predominant species in the Pt/TiC NWs, Pt/C and Pt/CFs. In addition, Fig. 4a, b and c shows that the Pt 4f<sub>5/2</sub> and 4f<sub>7/2</sub> peaks of Pt/TiC NWs both shift to higher binding energies (71.76 and 75.08 eV) relative to the Pt 4f<sub>5/2</sub> and 4f<sub>7/2</sub> peaks of Pt/C (71.34 and 74.64 eV) and Pt/CFs (71.71 and 75.07 eV). The XPS data is also listed in Table S1 (see ESI). The upshift of binding energy for Pt relative to Pt/C (Fig. 4d) confirms the strong electron interactions involving Pt and TiC NWs in the Pt/TiC NWs catalysts.<sup>5</sup> The electron interactions between Pt and TiC NWs alter the electronic states of Pt atoms and downshift the d-band center position,<sup>4</sup> thus resulting in the enhancement of the electrocatalytic activity and decrease the adsorption energy of CO on Pt. These results are in good agreement with CV results.

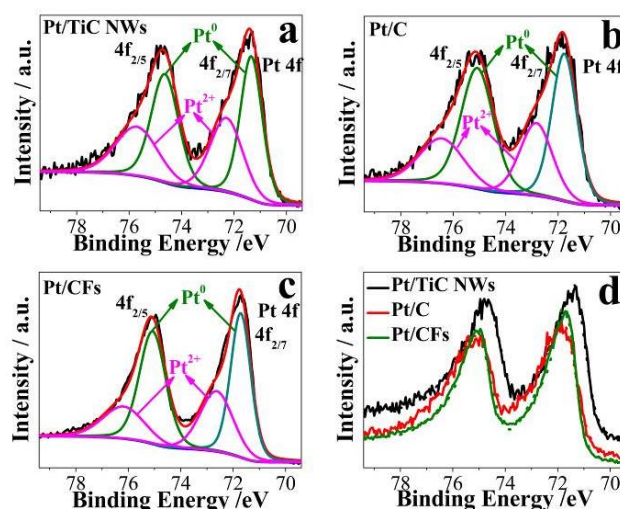


**Fig. 4** (a–c) XPS spectra of Pt 4f performed on the Pt/TiC NWs, Pt/C and Pt/CFs catalysts. (d) Comparison of the XPS spectra of Pt 4f orbital of the Pt/TiC NWs, Pt/C and Pt/CFs catalysts.

The ECSA of the catalysts can be calculated from hydrogen adsorption/desorption region after deduction of the double-layer region. Fig. 5 shows the CVs of the Pt/TiC NWs, Pt/C and Pt/CFs before and after 500 cycles in N<sub>2</sub>-saturated 0.5 M H<sub>2</sub>SO<sub>4</sub> aqueous solution.<sup>53,54</sup> All the CVs show the typical features corresponding to hydrogen adsorption/desorption, double-layer charging and oxide formation/reduction on the Pt surface. It is well known that a catalyst with larger ECSA usually possesses higher electrocatalytic activity.<sup>23, 55, 56</sup> The ECSA of the Pt/TiC NWs is estimated to be 203.83 m<sup>2</sup> g<sup>-1</sup>, much higher than that of the Pt/C (140.12 m<sup>2</sup> g<sup>-1</sup>) and Pt/CFs (16.96 m<sup>2</sup> g<sup>-1</sup>). The significantly larger value can be explained as following: (i) the XPS results verify (Fig. 4) the strong interaction between the Pt nanoparticles and the TiC NWs, which essentially prevents migration and agglomeration of Pt nanoparticles; (ii) unlike the Pt/C and Pt/CFs, the Pt crystallites are almost exposed on the surface of the TiC NWs, which provides more electrochemical active sites for MOR; (iii) the excellent electrical conductivity and unique 1D nanoarchitecture of the TiC NWs could facilitate electron transport along the long dimension and the two short dimensions provide short pathways for species. Additionally, after 500 cycles, no recordable loss of ECSA on Pt/TiC NWs (Fig. 5a) is observed, while ~43% and ~50% loss of ECSA on Pt/C (Fig. 5b) and Pt/CFs (Fig. 5c) are observed. That is the direct evidence that Pt/TiC NWs has superior stability in comparison with Pt/C and Pt/CFs. The improved stability of the Pt/TiC NWs catalyst might originate from TiC NWs, which processes better corrosion resistance and electrical conductivity,

preventing the growth of platinum particles under the testing conditions.

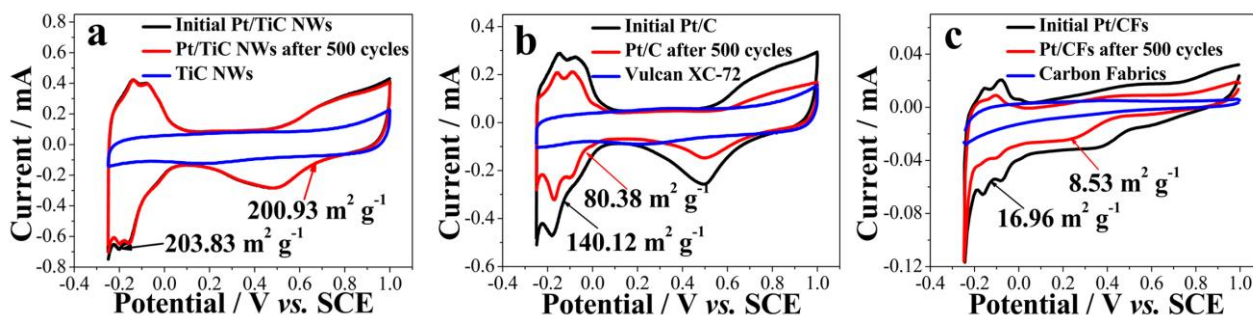


Fig. 5 CVs of (a) the Pt/TiC NWs, (b) Pt/C and (c) Pt/CFs before and after 500 cycles measured in solution of 0.5 M H<sub>2</sub>SO<sub>4</sub> at 50 mV s<sup>-1</sup>.

## 4 Conclusion

In conclusion, we have synthesized a new kind of bark-structured TiC nanowires (NWs) as an efficient support for Pt electrocatalysts. Our studies demonstrate that Pt/TiC NWs catalyst exhibited attractive electrocatalytic properties, such as higher electrochemical active surface area (ECSA), much improved electrocatalytic activity and long-term durability toward MOR in comparison with the Pt/C (Vulcan XC-72) catalyst and Pt/CFs catalyst. The unique structural features are greatly advantageous for enhancement of the MOR, because of the superior electrical conductivity, large surface area, fast transport and short diffusion paths for electroactive species and homogeneous loading of small platinum nanoparticles. Here, the use of TiC NWs as a catalyst support will not only open new and exciting possibilities for enhancing the performance of electrochemical activity, but also promote broader interest for the design of next-generation electrocatalysts and other electrocatalytic fields.

## Acknowledgements

This work was supported by National Natural Science Foundation of China (No. 20673100, 51172205 and 51002138), Natural Science Foundation of Zhejiang Province (LR13E020002 and LY13E020010) Qianjiang Project of Zhejiang Province (2010R10029) and New Century Excellent Talents in University (NCET 111079).

## References

- K. Yamamoto, T. Imaoka, W. J. Chun, O. Enoki, H. Katoh, M. Takenaga and A. Sonoi, *Nat Chem*, 2009, **1**, 397-402.
- S. Chu and A. Majumdar, *Nature*, 2012, **488**, 294-303.
- R. Y. Wang, C. Wang, W. B. Cai and Y. Ding, *Adv Mater*, 2010, **22**, 1845-+.
- H. H. Li, S. Zhao, M. Gong, C. H. Cui, D. He, H. W. Liang, L. Wu and S. H. Yu, *Angew Chem Int Edit*, 2013, **52**, 7472-7476.
- A. L. Wang, H. Xu, J. X. Feng, L. X. Ding, Y. X. Tong and G. R. Li, *J Am Chem Soc*, 2013, **135**, 10703-10709.
- X. M. Ma, H. Meng, M. Cai and P. K. Shen, *J Am Chem Soc*, 2012, **134**, 1954-1957.
- D. Strmcnik, M. Escudero-Escribano, K. Kodama, V. R. Stamenkovic, A. Cuesta and N. M. Markovic, *Nat Chem*, 2010, **2**, 880-885.
- M. K. Debe, *Nature*, 2012, **486**, 43-51.
- C. K. Poh, Z. Tian, J. Gao, Z. Liu, J. Lin, Y. P. Feng and F. Su, *J. Mater. Chem.*, 2012, **22**, 13643-13652.
- Z. Yao, M. Zhu, F. Jiang, Y. Du, C. Wang and P. Yang, *J. Mater. Chem.*, 2012, **22**, 13707-13713.
- H. Lv, T. Peng, P. Wu, M. Pan and S. Mu, *J. Mater. Chem.*, 2012, **22**, 9155-9160.
- Z. Y. Zhou, Z. Z. Huang, D. J. Chen, Q. Wang, N. Tian and S. G. Sun, *Angew. Chem., Int. Ed.*, 2010, **49**, 411-414.
- X. Yuan, X.-L. Ding, C.-Y. Wang and Z.-F. Ma, *Energy Environ. Sci.*, 2013, **6**, 1105-1124.
- Z. Qiu, H. Huang, J. Du, T. Feng, W. Zhang, Y. Gan and X. Tao, *J. Phys. Chem. C*, 2013, **117**, 13770-13775.
- Z. Chen, M. Waje, W. Li and Y. Yan, *Angew Chem Int Edit*, 2007, **46**, 4060-4063.
- B. Y. Xia, W. T. Ng, H. B. Wu, X. Wang and X. W. Lou, *Angew Chem Int Edit*, 2012, **51**, 7213-7216.
- Y. Shao, J. Liu, Y. Wang and Y. Lin, *J. Mater. Chem.*, 2009, **19**, 46-59.
- S. K. Meher and G. R. Rao, *Acs Catal.*, 2012, **2**, 2795-2809.
- X. L. Ji, K. T. Lee, R. Holden, L. Zhang, J. J. Zhang, G. A. Botton, M. Couillard and L. F. Nazar, *Nat Chem*, 2010, **2**, 286-293.
- K. G. Nishanth, P. Sridhar, S. Pitchumani and A. K. Shukla, *Ecs Transactions*, 2010, **33**, 2027-2034.
- R. Dhiman, S. N. Stamatini, S. M. Andersen, P. Morgen and E. M. Skou, *J. Mater. Chem. A*, 2013, **1**, 15509-15516.
- R. Ganesan and J. S. Lee, *Angew Chem Int Edit*, 2005, **44**, 6557-6560.
- Z. Yan, H. Wang, M. Zhang, Z. Jiang, T. Jiang and J. Xie, *Electrochim. Acta*, 2013, **95**, 218-224.
- J. Zang, L. Dong, Y. Jia, H. Pan, Z. Gao and Y. Wang, *Appl. Catal., B-Environ.*, 2014, **144**, 166-173.
- W. T. Grubb and D. W. McKee, *Nature*, 1966, **210**, 192-194.
- X. Y. Tao, Y. P. Li, J. Du, Y. Xia, Y. C. Yang, H. Huang, Y. P. Gan, W. K. Zhang and X. D. Li, *J. Mater. Chem.*, 2011, **21**, 9095-9102.
- M. R. Lukatskaya, O. Mashtalir, C. E. Ren, Y. Dall'Agnese, P. Rozier, P. L. Taberna, M. Naguib, P. Simon, M. W. Barsoum and Y. Gogotsi, *Science*, 2013, **341**, 1502-1505.
- X. H. Xia, J. P. Tu, Y. Q. Zhang, X. L. Wang, C. D. Gu, X. B. Zhao and H. J. Fan, *Acs Nano*, 2012, **6**, 5531-5538.
- X. H. Xia, J. P. Tu, Y. Q. Zhang, J. Chen, X. L. Wang, C. D. Gu, C. Guan, J. S. Luo and H. J. Fan, *Chem Mater*, 2012, **24**, 3793-3799.
- X. H. Xia, J. P. Tu, Y. J. Mai, X. L. Wang, C. D. Gu and X. B. Zhao, *J. Mater. Chem.*, 2011, **21**, 9319-9325.

31. W. Li, Y. Bai, F. J. Li, C. Liu, K. Y. Chan, X. Feng and X. H. Lu, *J. Mater. Chem.*, 2012, **22**, 4025-4031.
32. T. Xue, Z. P. Sun, L. Wei, X. Wang and J.-M. Lee, *Int. J. Hydrogen Energy*, 2013, **38**, 2754-2759.
33. Y. Y. Chu, Z. B. Wang, J. Cao, D. M. Gu and G. P. Yin, *Fuel Cells*, 2013, **13**, 380-386.
34. H. B. Liao and Y. L. Hou, *Chem Mater*, 2013, **25**, 457-465.
35. S. J. Guo and E. K. Wang, *Accounts Chem Res*, 2011, **44**, 491-500.
36. S. Du, *Int. J. Low-Carbon Tech.*, 2012, **7**, 44-54.
37. X. Y. Tao, J. Du, Y. C. Yang, Y. P. Li, Y. Xia, Y. P. Gan, H. Huang, W. K. Zhang and X. D. Li, *Cryst Growth Des*, 2011, **11**, 4422-4426.
38. J. Du, Y. C. Yang, Z. Fan, Y. Xia, X. J. Cheng, Y. P. Gan, H. Hang, L. X. Dong, X. D. Li, W. K. Zhang and X. Y. Tao, *J Alloy Compd*, 2013, **560**, 142-146.
39. X. Tao, J. Du, Y. Li, Y. Yang, Z. Fan, Y. Gan, H. Huang, W. Zhang, L. Dong and X. Li, *Adv. Energy Mater.*, 2011, **1**, 534-539.
40. B. Fang, N. K. Chaudhari, M. S. Kim, J. H. Kim and J. S. Yu, *J Am Chem Soc*, 2009, **131**, 15330-15338.
41. G. Cui, P. K. Shen, H. Meng, J. Zhao and G. Wu, *J Power Sources*, 2011, **196**, 6125-6130.
42. Z. Tang and G. Lu, *Appl. Catal., B-Environ.*, 2008, **79**, 1-7.
43. B. Wu, Y. Kuang, X. Zhang and J. Chen, *Nano Today*, 2011, **6**, 75-90.
44. A. X. Yin, X. Q. Min, Y. W. Zhang and C. H. Yan, *J Am Chem Soc*, 2011, **133**, 3816-3819.
45. Z. Liu, Q. Shi, F. Peng, H. Wang, R. Zhang and H. Yu, *Electrochem. Commun.*, 2012, **16**, 73-76.
46. C. Pan, L. Qiu, Y. Peng and F. Yan, *J. Mater. Chem.*, 2012, **22**, 13578-13584.
47. Y. Guo, C. Hu, L. Yang, Z. Bai, K. Wang and S. Chao, *Electrochem. Commun.*, 2011, **13**, 886-889.
48. Y. Wang, T. S. Nguyen, X. Liu and X. Wang, *J Power Sources*, 2010, **195**, 2619-2622.
49. B. Wu, D. Hu, Y. Kuang, B. Liu, X. Zhang and J. Chen, *Angew Chem Int Edit*, 2009, **48**, 4751-4754.
50. Y. Zhao, Y. Wang, X. Cheng, L. Dong, Y. Zhang and J. Zang, *Carbon*, 2014, **67**, 409-416.
51. Y. Ou, X. Cui, X. Zhang and Z. Jiang, *J. Power Sources*, 2010, **195**, 1365-1369.
52. Z. C. Ju, N. Fan, X. C. Ma, J. Li, X. J. Ma, L. Q. Xu and Y. T. Qian, *J Phys Chem C*, 2007, **111**, 16202-16206.
53. B. Wu, D. Hu, Y. Yu, Y. Kuang, X. Zhang and J. Chen, *Chem. Commun.*, 2010, **46**, 7954-7956.
54. Y. Kuang, Y. Cui, Y. Zhang, Y. Yu, X. Zhang and J. Chen, *Chem. Eur. J.*, 2012, **18**, 1522-1527.
55. J. Xu, G. Fu, Y. Tang, Y. Zhou, Y. Chen and T. Lu, *J. Mater. Chem.*, 2012, **22**, 13585-13590.
56. R. Wang, H. Wang, B. Wei, W. Wang and Z. Lei, *Int. J. Hydrogen Energy*, 2010, **35**, 10081-10086.